Polish Journal of Medical Physics and Engineering
The Journal of Polish Society of Medical Physics
ISSN 1898-0309, doi: 10.2478/pjmpe-2025-0035

December 2025
Vol 31, Issue 4

Scientific Paper

Investigating the Dose Parameters of Low-Level Laser Therapy to Optimize Therapeutic Efficacy

Kawthar Shurrab [1,*]

[1]*Higher Institute for Laser Research and Applications, Damascus University, Damascus, Syrian Arab Republic*
**Corresponding author: Kawthar Shurrab; kawthar.shurrab@damascusuniversity.edu.sy*

(received 1 May 2025; revised 30 June 2025; accepted 26 September 2025)

Abstract

Introduction: Low-level laser therapy (LLLT), also known as photobiomodulation, has emerged as a promising therapeutic option for various medical applications, including pain management and wound healing. This study aims to investigate the dose parameters of LLLT to optimize therapeutic efficacy.

Materials and Methods: We utilized Finite Element Analysis within the COMSOL Multiphysics software package to model light-tissue interactions and refine dosing protocols. Lasers with wavelengths of 660 nm, 780 nm, and 808 nm were selected due to their widespread use in therapy. Additionally, we examined several factors that impact the effectiveness of the treatment. Key parameters considered include energy, energy density, power, power density, irradiation time, and tissue penetration depth.

Results: The recommended stimulation time should not exceed six minutes (480 seconds) at a power density of 15.62 mW/cm². However, if the power density is reduced to a maximum of 3.10 mW/cm², the stimulation time can be safely extended to 10 minutes (600 seconds) without causing undesirable thermal effects, as long as the tissue temperature does not exceed 40°C during the extended stimulation.

It is important to note that the dose applied to the surface of the tissue significantly decreases as it penetrates deeper. The average energy loss is approximately 11% per millimetre of tissue. Our simulations indicate that effective doses range from 0.38 J/cm² to 9.37 J/cm² while maintaining safe tissue temperatures, which are consistent with WALT recommendations.

Conclusion: Our findings help identify factors influencing stimulation, guiding therapists to standardize treatment parameters such as wavelength, exposure time, and dosages measured in joules, watts, W/cm², and J/cm² for consistency and safety across studies.

Keywords: Low-Level Laser Therapy; Doses; Photobiomodulation; Medical Applications; Treatment

Introduction

Low-level Laser Therapy (LLLT), also referred to as photobiomodulation, employs low-intensity laser light to stimulate cellular activities and enhance healing mechanisms. Specifically, it is used to promote tissue regeneration, alleviate inflammation, and provide pain relief[1,2].

LLLT primarily works by activating cytochrome c oxidase, an essential enzyme in the mitochondrial respiratory chain. This activation boosts cellular respiration and ATP production, thus supplying more energy for cellular repair and regeneration. The laser light is absorbed by cellular photoreceptors, initiating photochemical reactions that stimulate cellular functions[3]. This process aligns with the Grotthuss-Draper law, which posits that light must be absorbed by a chemical substance to trigger a photochemical reaction[4,5]. According to Posten et al.,[6] the characteristics of low-level lasers include: a) Power output ranging from 0.001 to 0.1 Watts; b) Wavelengths spanning from 300 to 10,600 nm; c) Pulse rates varying from continuous (0) up to 5000 Hertz (cycles per second); d) Intensity levels of 0.15 to 10 mW/cm², and dosages between 0.01 to 100 J/cm² [1,6].

Effective LLLT dosing relies on several critical parameters. The wavelength determines the specific depth of tissue penetration and interaction type, directly impacting therapeutic efficacy. Power density or energy density refers to the amount of laser power delivered per unit area, significantly influencing cellular stimulation (Chow et al., 2009)[2,7]. Exposure time, which is the duration of laser exposure, dictates the overall energy delivered to the tissue and is crucial for optimizing

Authors' contribution: A – Research concept and design, B – Collection and/or assembly of data, C – Data analysis and interpretation, D – Writing the article, E – Critical revision of the article, F – Final approval of the article.

therapeutic outcomes (Hamblin, 2016)[8]. Finally, the frequency of treatment, referring to the number of treatment sessions and their intervals, can profoundly affect the effectiveness of LLLT in various medical applications[9,10]. Although extensive research has been conducted on the efficacy of low-energy lasers, there remains a significant gap in establishing optimal treatment parameters and a lack of information, particularly regarding dose determination. The inconsistent findings across various studies have limited the broader adoption of low-level laser therapy. However, LLLT continues to be utilized in clinical practice across various fields to treat numerous conditions. The critical challenge is identifying the precise dosages needed to enhance its efficiency[6,11-13].

Finite Element Method (FEM) software, like COMSOL Multiphysics, is essential for simulating the interaction of laser light with biological tissues and optimizing dosages to enhance therapeutic outcomes[14]. FEM tools model laser energy distribution and absorption within tissues, predicting temperature changes to ensure thermal effects remain safe while maximizing the benefits of LLLT[15]. By simulating various scenarios, researchers can determine the optimal combination of laser power, exposure time, and treatment frequency for different medical applications. For example, COMSOL Multiphysics can model how laser light penetrates tissue layers, allowing for adjustments in treatment protocols based on specific patient needs[16]. This research is crucial in understanding photon distribution and absorption, as well as examining potential thermal effects during stimulation, to optimize treatment parameters such as wavelength, power, power density, energy, energy density, and exposure time. This optimization improves dosage and enhances healing. Lasers with wavelengths of 660, 780, and 808 nm were selected for their widespread use in stimulation. This study is a valuable reference for researchers investigating low-level laser technology, as these parameters have not been explored previously due to their absence or lack in most studies.

Materials and Method

This study aimed to analyze the temperature distribution in human tissue under varying red to near-infrared laser irradiation to estimate the thermal range and dose distribution associated with cellular activation during Low-Level Laser Therapy. The research focused on identifying the optimal parameters for treatment, specifically examining factors such as power, power density, energy, energy density, and treatment duration. The study utilized lasers with wavelengths of 660 nm, 780 nm, and 808 nm and had an effective laser area of 32 cm^2, commonly used in LLLT. To conduct the simulations, a model was developed based on the Finite Element Method (FEM) using COMSOL Multiphysics 6.1 software, incorporating Pennes' bio-heat transfer equation

Bioheat transfer Equation

The bio-heat equation, commonly referred to as Pennes' bioheat transfer equation, is utilized to calculate the propagation of laser dose through biological tissue in low-level laser therapy (LLLT). This equation models heat transfer within tissues by considering various factors, including laser energy absorption, blood perfusion, and metabolic heat generation. By solving this equation, researchers can predict temperature distributions and thermal effects, which helps inform the dose distribution within tissues. This understanding is essential for optimizing the parameters of laser therapy, ensuring that treatments are both safe and effective[17-19]:

$$\delta_{ts}\rho C\frac{\partial T}{\partial t}+\nabla.\left(-K\nabla T\right)=\rho_b C_b\omega_b\left(T_b-T\right)+Q_{met}+Q_{Laser} \quad (1)$$

Where δ_{ts} represents the time ratio (the default value is 1), ρ is a density of tissue (kg/m^3), C signifies the specific heat capacity of the tissue (J/(kg·K)), T is a temperature (°C), K is a thermal conductivity of tissue (W/(m·K)), ρ_b is a density of blood (kg/m^3), C_b is a specific heat of blood (J/(kg·K)), ω_b is a volumetric perfusion rate (s^{-1}), T_b is a temperature of arterial blood (°C), Q_{met} is a metabolic heat source (W/m^3), Q_{Laser} is a laser heat source (W/m^3).

LLLT Propagation Calculation

While the tissue absorbs a fraction of the incident laser light, the remaining light will be scattered, reflected, or refracted. Here, we suppose that the light source is a Gaussian beam, and we can define Q_{Laser} in Eq. 1 as follows[20,21]:

$$Q_{Laser}=\mu_a\left[\left(1-R\right)\frac{2P}{\pi\omega_0^2}\exp\left(\frac{-2r^2}{\omega_0^2}\right)\exp\left(-\mu_t z\right)f\left(t\right)\right] \quad (2)$$

where:

μ_a is the absorption coefficient (1/mm), R is the reflectance at normal incidence, P is the laser power (mW), ω_0 is the beam radius at the irradiation surface (mm), and $\mu_t=\mu_a+\mu_s$ represents the total attenuation coefficient including both absorption and scattering (μ_s,1/mm). and term $f(t)$ denotes a time dependent function described later (see Eq. 4).

The exponential term $\exp(-\mu_t z)$ accounts for the attenuation of light with penetration depth (z), accounting for both absorption and scattering effects for each layer. As laser light penetrates the layers of skin, energy decreases due to both scattering and absorption. The extent of this attenuation depends strongly on wavelength; for instance, longer wavelengths (e.g., 808 nm) penetrate deeper than shorter ones (e.g., 660 nm), consistent with optical properties reported in **Table 1**.

Human skin is composed of three layers: epidermis, dermis, and subcutaneous tissue, each with distinct thicknesses and optical characteristics. Due to variations in reported literature values[22-25], average values are used for modeling. The depths of the epidermis, dermis, and subcutaneous tissue are denoted as z_1, z_2, and z_3, respectively (see **Figure 1** and **Table 1**).

The heat source terms for the epidermis and dermis layers can be written as:

$$Q_{epidemis}=\mu_{a1}*\left[\left(1-R\right)\frac{2P}{\pi\omega_0^2}\exp\left(\frac{-2r^2}{\omega_0^2}\right)\exp\left(-\mu_{s1}z-\mu_{a1}z\right)*f\left(t\right)\right] \quad (3)$$

$$Q_{dermis} = \mu_{a2} * \left[\frac{2P}{\pi\omega_0^2} \exp\left(\frac{-2r^2}{\omega_0^2}\right) \exp\left(-\mu_{s1} z_1 - \mu_{s2}(z - z_1) - \right.\right. \\ \left.\left. - \mu_{a1} z_1 - \mu_{a2}(z - z_1)\right) * f(t) \right] \quad (4)$$

As the heat source varies over time, it should be multiplied by a time dependent function.

$$f(t) = \exp\left(-(t/\tau)^2\right) \quad (5)$$

Where t represents the calculation time (s), while τ is the total irradiation duration (s). This time-dependent function modulates all heat source expressions to reflect pulsed or continuous exposure

Simulation Model

The simulation employs a 2D model that represents skin layers and is implemented using the FEM software COMSOL Multiphysics 6.1. To improve computational efficiency, a 2D axisymmetric model was created, with the r-axis indicating the cylinder radius and the z-axis representing depth in the multilayer skin tissue. **Figure 1** illustrates the geometric model comprising three layers: z_1 epidermis, z_2 dermis, and z_3 subcutaneous tissue. The bioheat equation, shown in Eq. 1, is employed to calculate heat transfer from a continuous-wave laser, Gaussian beam with wavelengths of 660, 780, and 808 nm (Konftec Laser, emLas®-650, for LLLT), and laser effective area is 32 cm². The thickness of each layer and its refractive index (n), thermal properties, and optical parameters are summarized in **Table 1**[24-27].

The density of blood is 1060 kg/m³, its heat capacity is 3770 J/(kg·K), and its Blood perfusion rate is 0.5 s^{-1} [26]. The arterial blood temperature is assumed to be 37°C. In Eq. 2, the reflectance $R = \frac{(n-1)^2}{(n+1)^2}$ [28,29]

In this simulation model, the initial conditions and four boundary conditions are defined as follows:

1. The line of axial symmetry is set to be thermally insulated.
2. The initial temperature of the tissue is typically set to the normal body temperature, approximately 37°C, while the external temperature is set at 28°C.
3. A laser flux boundary condition is applied at the laser irradiation surface to simulate the entry of laser energy into the skin.
4. A convective heat transfer boundary condition is applied at the outer surface of the tissue to account for heat loss to the surrounding environment.
5. The boundaries between the inner layers are defined to maintain continuity, and we assume the initial temperature of the other boundaries is 37.2°C[19,30].

It is important to note that we assigned an internal tissue temperature of approximately 37°C and an ambient external temperature of 28°C. These values are commonly used in numerical simulations for standardization and comparability[19,30]. However, the actual skin surface temperature varies based on anatomical location and environmental factors. Some studies indicate that surface temperatures are generally lower than core temperatures, ranging from 28°C to 36°C, depending on the body region, humidity, airflow, vascularity, and clothing[31,32]. For instance, distal areas, such as the feet and hands, often exhibit temperatures as low as 28-32°C, while central regions, like the abdomen, may maintain higher values, approaching 36°C.

To calculate the dose of laser energy in joules per square centimeter (J/cm²), we can use the following formula[33,34]:

$$Dose\left(\frac{\mathrm{J}}{\mathrm{cm}^2}\right) = \left(\frac{Power(\mathrm{W})}{Area(\mathrm{cm}^2)}\right) * Time(\mathrm{s}) \quad (6)$$

Table 1. The thermal properties and optical parameters.

Wavelength (nm)	Epidermis		Dermis		Subcutaneous tissue	
	μ_a (1/mm)	μ_s (1/mm)	μ_a (1/mm)	μ_s (1/mm)	μ_a (1/mm)	μ_s (1/mm)
660[25]	0.94	5.55	0.07	3.06	0.07	1.72
780[25]	0.68	5.18	0.06	2.63	0.06	1.65
808[25]	0.49	3.98	0.06	2.30	0.06	1.37
Thickness (mm)[26]	0.04-0.16 (0.08)		1.6-2.8 (2.0)		10	
Refractive index n[27]	1.45 – 1.55		1.38 – 1.42		1.34 – 1.36	
Thermal conductivity (W/m·°C)[26]	0.21-0.26 (0.24)		0.37-0.52 (0.45)		0.16-021 (0.19)	
Specific heat ($Jkg^{-1}k^{-1}$)[26]	3578-3600 (3590)		3200-3400 (3330)		2300-3060 (2500)	
Density (kg/m^3)[26]	1200		1200		1000	
Water content (%)[26]	70		70		20	

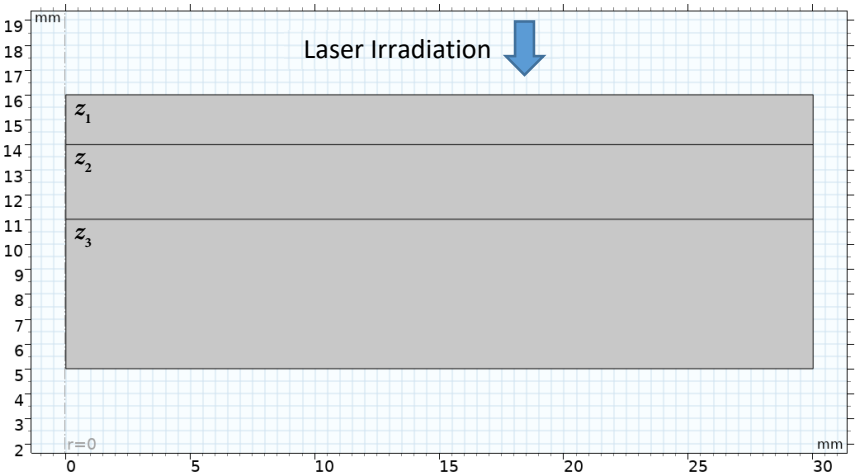

Figure 1. Schematic of the three layers-skin model: z_1 is an epidermis, z_2 is a dermis, z_3 is a subcutaneous tissue.

Where Power (W) is the laser power in W or mW, Area (cm^2) is the area over which the laser is applied in square centimeters, and time (s) is the duration of laser application in seconds.

Results and Discussions

In this article, we performed finite element simulations to analyze how laser dose is distributed and varies within skin tissue during stimulation at different levels of laser power, power density, and exposure times. We also investigated the potential temperature distribution in the tissue during stimulation using various wavelengths that are commonly used in photobiomodulation. The results are presented in **Table 2**, **Figure 2**, **Figure 3**, and **Figure 4**.

Table 2 demonstrates that as power and energy density increase alongside longer irradiation durations, the maximum temperature of the treated tissue also rises. The temperatures listed represent the maximum surface tissue temperatures recorded at the end of each corresponding irradiation time. These durations, specifically 2, 4, 6, 8, and 10 minutes, were selected based on their frequent use in clinical protocols reported in the literature. This temporal framework allows for direct comparison with therapeutic norms and ensures that simulation outputs remain relevant to practice.

Table 2. The surface dose values at different wavelengths.

Power (mW)	**100**	**250**	**500**	**700**	**1000**
Laser effective area (cm^2)	**32**	**32**	**32**	**32**	**32**
660 Wavelength (nm)					
Power density (mW/cm^2)	3.10	7.81	15.62		
*Tissue Temperature (°C)	38	38.8	40		
Therapy time (min)	Joule density (J/cm^2)				
2	0.38	0.93	1.87		
4	0.75	1.87	3.75		
6	1.12	2.81	5.63		
8	1.50	3.75	7.50		
10	1.88	4.69	9.37		
780 Wavelength (nm)					
Power density (mW/cm^2)	3.10	7.81	15.62	21.87	31.25
*Tissue Temperature (°C)	38	38.8	40	41.2	42.9
Therapy time (min)	Joule density (J/cm^2)				
2	0.37	0.93	1.87	2.63	3.75
4	0.75	1.87	3.75	5.25	7.50
6	1.12	2.81	5.63	7.87	11.25
8	1.50	3.75	7.50	10.50	15
10	1.88	4.69	9.37	13.13	18.75
808 Wavelength (nm)					
Power density (mW/cm^2)	3.10	7.81	15.62	21.87	31.25
*Tissue Temperature (°C)	38	38.8	40.1	41.3	42.9
Therapy time (min)	Joule density (J/cm^2)				
2	0.37	0.93	1.87	2.63	3.75
4	0.75	1.87	3.75	5.25	7.50
6	1.12	2.81	5.63	7.87	11.25
8	1.50	3.75	7.5	10.50	15
10	1.87	4.69	9.37	13.13	18.75

*Temperature values represent the maximum tissue surface temperature at the end of each therapy duration.

Highlighting the endpoint temperatures at each time interval is critical for evaluating the thermal safety of each dosage, particularly in ensuring that tissue temperatures remain below the threshold of 40°C during photobiomodulation treatments.

For a wavelength of 660 nm, as power increases from 100 mW to 500 mW, the power density increases from 3.10 mW/cm^2 to 15.62 mW/cm^2, resulting in a tissue temperature rise from 38°C to 40°C.

At 780 nm, power densities vary from 3.10 mW/cm^2 to 31.25 mW/cm^2 as power reaches up to 1000 mW, leading to tissue temperatures that range from 38°C to 42.9°C. Similarly, for an 808 nm wavelength, power densities also range from 3.10 mW/cm^2 to 31.25 mW/cm^2, with tissue temperatures reaching from 38°C to 43°C.

It is important to note that tissue temperature can exceed 40°C during extended stimulation periods, so caution is necessary even with Low-Level Laser Therapy (LLLT). The recommended stimulation time for the skin should not exceed six minutes (480 seconds) at a power density of 15.62 mW/cm^2. However, when using a power density of 3.10 mW/cm^2, the stimulation time can be extended to 10 minutes (600 seconds) without causing undesirable heat effects, as shown in **Figure 2**.

Furthermore, when power density is increased while keeping irradiation time constant, the skin temperature rises linearly. This observation corresponds with the simulation outcomes reported by Vitkaya[35].

Figure 3 illustrates the influence of penetration depth in LLLT. The crucial point is that the dose of laser stimulation decreases as it penetrates deeper into the tissue, resulting in lower energy density at greater depths. It demonstrates how the dose distribution varies with different energy densities: (a) 3.10 mW/cm^2, (b) 7.81 mW/cm^2, (c) 15.62 mW/cm^2, (d) 21.87 mW/cm^2, and (e) 31.25 mW/cm^2, all based on an irradiation time of 480 s. While a higher power density results in a greater initial dose at the surface, it also leads to a more rapid decline in dose as it penetrates deeper into the tissue. This observation underscores the necessity of carefully calibrating power density to achieve the desired therapeutic effect at specific tissue depths while ensuring both safety and efficacy. Interestingly, lower doses are often more effective in stimulating deeper tissue layers compared to higher doses. This is especially noticeable at a power level of 100 mW and a power density of 3.10 mW/cm^2, where the dose penetrates deeper into the tissue, as illustrated by the red color in **Figure 3a**. In contrast, higher doses show less penetration when measured at the same time and wavelength.

At lower power densities, the photon fluence rate is reduced, which promotes more uniform light distribution and allows photons to penetrate deeper into tissue before undergoing significant absorption or scattering. In this context, although the dermis has a lower absorption coefficient compared to the melanin-rich epidermis, its reduced attenuation enables a greater number of photons to reach deeper layers. As a result, chromophores located within the dermis, such as hemoglobin and water, can still effectively absorb the transmitted light. This interplay between scattering and residual ab-

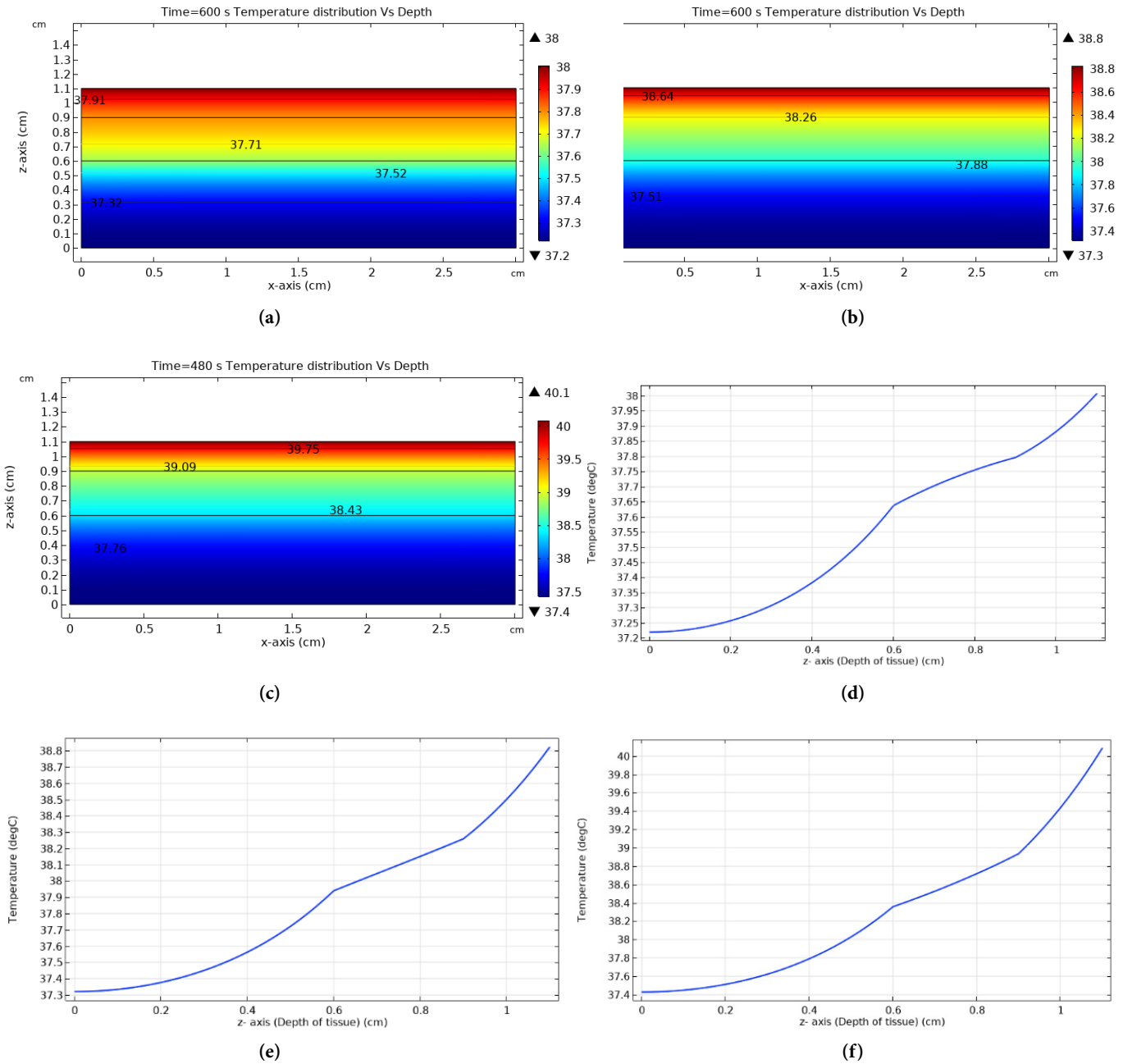

Figure 2. The 2D temperature distribution within the skin for power density a) 3.10 mW/cm², b) 7.81 mW/cm² at t = 600 s, and c) 15.62 mW/cm² at 480 s; and temperature versus depth of tissue (d) at 600 s, e) at 600 s, and (f) 480 s.

sorption may lead to the emergence of a secondary subsurface peak in energy deposition, particularly in regions where these interactions are optimally balanced.

This observation supports the Arndt-Schulz Law, which suggests that lower doses can be more effective than higher doses in eliciting a physiological response, a finding that is consistent with numerous other studies. This confirms the validity of our simulation[33,36-38].

Additionally, as shown in **Figure 4**, we observed that the loss of energy density and power density ranges between 9% and 14% per millimeter across different tissue layers. This variation is primarily influenced by the optical absorption and scattering coefficients of each layer, with superficial layers (such as the epidermis) exhibiting higher attenuation, while deeper dermal and subcutaneous tissues exhibit lower relative losses[38,39]. This results in an average attenuation of approximately 11% per millimeter of tissue depth. The observed behavior follows an exponential decay model, which can be expressed as:

$$Loss\ Factor = (1-0.011)^{x} \quad (7)$$

Where x represents the depth of the tissue in mm, measured from the interior of the tissue (z = 0 cm) toward the skin surface (z = 1.1 cm), where LLLT is applied.

It has been observed that changing the duration of irradiation does not impact the power density, which remains constant. Therefore, measuring the dose in joules per square centimeter is essential, and calculating the dose in joules is the most effective approach. This approach helps explain the discrepancies found in previous studies, as one contributing factor is the omission of dose measurements in joules[36,40].

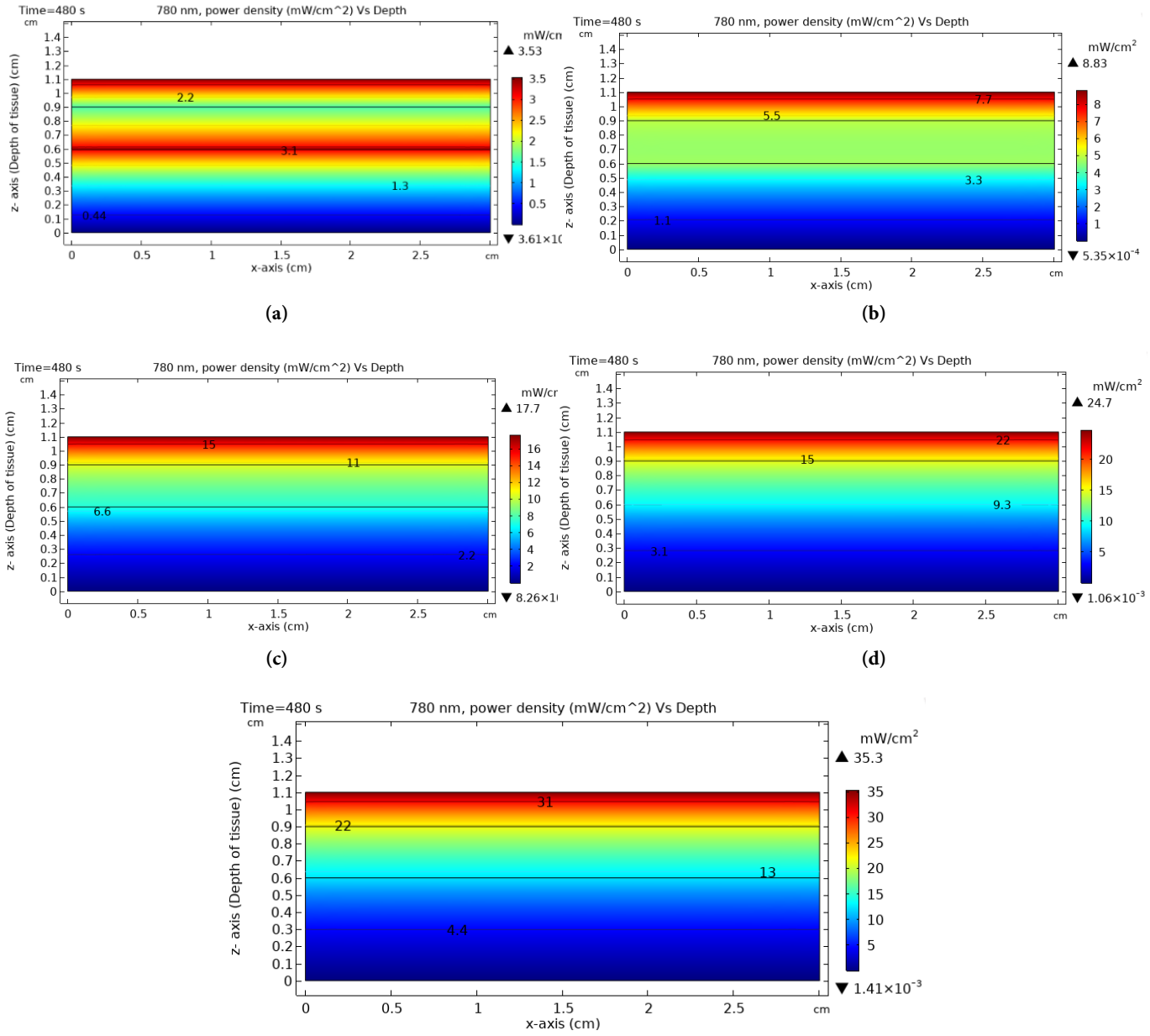

Figure 3. 2D Power density distribution within skin tissue at 780 nm, and t =480 s for different power density (a) 3.10 mW/cm², (b) 7.81 mW/cm², (c) 15.62 mW/cm², (d) 21.87 mW/cm², and (e) 31.25 mW/cm².

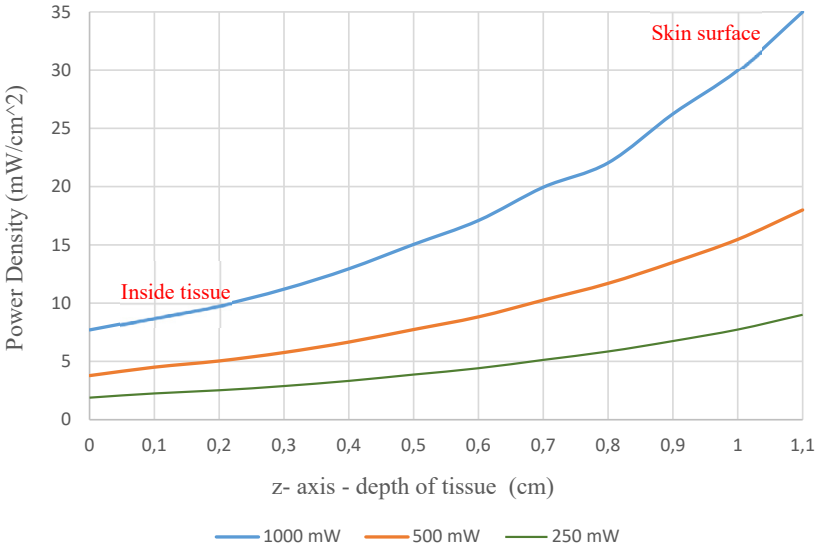

Figure 4. Power density as a function of tissue depth, from the skin surface (z = 1.1 cm) to the interior (z = 0 cm) during LLLT. An exponential decrease in power density is observed, with average attenuation of approximately 11% per millimeter. The figure illustrates the decrease at different power values.

This is significant clinically as the J/cm² is confused when comparing dosages between protocols, where the resultant dose in J/cm² could result from several different treatment options.

For example, the energy density of 1.12 J/cm² from **Table 2** can be delivered in different ways:

1) Using 100 mW for 6 minutes with a laser effective area of 32 cm², this results in a total of 36 J.
2) Using 50 mW for 6 minutes with a laser effective area of 16 cm², this totals 18 J.

This means that one patient received twice the total amount of energy compared to the other patient.

It is recommended that therapists using LLLT provide all dosage parameters in Joules, Watts, W/cm², and J/cm². This standardization will enhance dosage consistency and allow for comparison across different treatment regimes.

The maximum dose for Low-Level Laser Therapy LLLT varies by treatment protocol and condition. According to the World Association for Laser Therapy (WALT), recommended dosages range from 2 J/cm² to 10 J/cm², with 4 J/cm² to 8 J/cm² being the most common[33,34]. Our simulations support this, showing doses from 0.38 J/cm² to 9.37 J/cm², while ensuring tissue temperature should not exceed 40°C for extended stimulation.

Limitations

While this simulation offers valuable insights into thermal dose behavior in LLLT, several limitations must be acknowledged. First, the optical and thermal properties of skin tissues can vary widely among individuals due to factors such as pigmentation, hydration, and age. Our model employs average values from the literature, which may not capture the full range of biological variability.

Second, although Pennes' bioheat equation incorporates blood perfusion, our simulation assumes constant perfusion rates and arterial temperature. In vivo, perfusion can change dynamically in response to heat or tissue activation, potentially influencing temperature distribution during therapy.

Third, the model uses simplified, uniform boundary conditions to ensure computational efficiency. While this improves consistency, it does not fully replicate real-world conditions such as environmental heat exchange or patient-specific skin geometry.

Despite these limitations, our approach provides a robust and transparent simulation of LLLT dose parameters and thermal safety, forming a foundation for future work that incorporates more personalized and dynamic physiological variables.

Conclusion

Low-Level Laser Therapy (LLLT) demonstrates strong potential across medical fields, with computational simulations offering valuable insight into optimizing dose parameters. Our findings suggest that maintaining energy densities between 0.38 – 9.37 J/cm², without exceeding tissue temperatures of 40°C, ensures therapeutic safety and efficacy. Optimal stimulation spans 480 s at 7.50 J/cm² or up to 600 s at 1.88 J/cm². Energy attenuation with tissue depth follows an exponential trend, averaging 11% per millimeter. Standardizing these parameters will enhance treatment consistency and guide future research toward more effective clinical applications.

Conflicts of Interest

The authors declare no conflicts of interest.

Funding

The authors received no specific funding for this work.

References

1. Farivar S, Malekshahabi T, Shiari R. Biological effects of low level laser therapy. J Lasers Med Sci. 2014;5(2):58-62.
2. Chow RT, Johnson MI, Lopes-Martins RA, Bjordal JM. Efficacy of low-level laser therapy in the management of neck pain: a systematic review and meta-analysis of randomised placebo or active-treatment controlled trials. The Lancet. 2009;374(9705):1897-1908. doi:10.1016/s0140-6736(09)61522-1
3. de Freitas LF, Hamblin MR. Proposed Mechanisms of Photobiomodulation or Low-Level Light Therapy. IEEE J Select Topics Quantum Electron. 2016;22(3):348-364. doi:10.1109/jstqe.2016.2561201
4. Oxford Reference. Grotthuss-Draper law. In Oxford Reference. Retrieved from: https://www.oxfordreference.com/abstract/10.1093/acref/9780198841227.001.0001/acref-9780198841227-e-1945
5. Chung H, Dai T, Sharma SK, Huang YY, Carroll JD, Hamblin MR. The Nuts and Bolts of Low-level Laser (Light) Therapy. Ann Biomed Eng. 2011;40(2):516-533. doi:10.1007/s10439-011-0454-7
6. Posten W, Wrone DA, Dover JS, Arndt KA, Silapunt S, Alam M. Low-Level Laser Therapy for Wound Healing. Dermatologic Surgery. 2005;31(3):334-340. doi:10.1097/00042728-200503000-00016
7. Andrade F do S da SD, Clark RM de O, Ferreira ML. Effects of low-level laser therapy on wound healing. Rev Col Bras Cir. 2014;41(2):129-133. doi:10.1590/s0100-69912014000200010
8. Hamblin MR. Mechanisms and applications of the anti-inflammatory effects of photobiomodulation. AIMS Biophysics. 2017;4(3):337-361. doi:10.3934/biophy.2017.3.337
9. Naeser MA, Martin PI, Ho MD, et al. Transcranial, Red/Near-Infrared Light-Emitting Diode Therapy to Improve Cognition in Chronic Traumatic Brain Injury. Photomedicine and Laser Surgery. 2016;34(12):610-626. doi:10.1089/pho.2015.4037

10. Mansouri V, Arjmand B, Rezaei Tavirani M, Razzaghi M, Rostami-Nejad M, Hamdieh M. Evaluation of Efficacy of Low-Level Laser Therapy. J Lasers Med Sci. 2020;11(4):369-380. doi:10.34172/jlms.2020.60
11. Taylor DN, Winfield T, Wynd S. Low-Level Laser Light Therapy Dosage Variables vs Treatment Efficacy of Neuromusculoskeletal Conditions: A Scoping Review. Journal of Chiropractic Medicine. 2020;19(2):119-127. doi:10.1016/j.jcm.2020.06.002
12. da Fonseca A de S. Is there a measure for low power laser dose? Lasers Med Sci. 2018;34(1):223-234. doi:10.1007/s10103-018-2676-5
13. Shurrab K, Alzghayar JN. Low-level laser therapy for skin rejuvenation: A safe and effective solution baked by data and visual evidence. J of Cosmetic Dermatology. 2024;23(10):3234-3240. doi:10.1111/jocd.16404
14. Sannyal M, Mukaddes AMM, Rahman MdM, Mithu MAH. Analysis of the effect of external heating in the human tissue: A finite element approach. Polish Journal of Medical Physics and Engineering. 2020;26(4):251-262. doi:10.2478/pjmpe-2020-0030
15. Freddo AL, Hauser EB, de Castro VV, Noritomi PY, de Almeida AS, de Oliveira MG. Finite Element Analysis of Masticatory Stress on Neoformed Bone Tissue After Distraction Osteogenesis and Low-Level Laser Therapy: A Pilot Study. Photomedicine and Laser Surgery. 2014;32(8):429-436. doi:10.1089/pho.2013.3671
16. Shurrab K, Sayem El-Daher M. Potential Thermal Effect of Stimulating Brain Tissue during Low Level Laser Therapy. J-BPE. Published online November 6, 2023:040303. doi:10.18287/jbpe23.09.040303
17. Ostadhossein R, Hoseinzadeh S. The solution of Pennes' bio-heat equation with a convection term and nonlinear specific heat capacity using Adomian decomposition. J Therm Anal Calorim. 2022;147(22):12739-12747. doi:10.1007/s10973-022-11445-x
18. Kengne E, Lakhssassi A, Vaillancourt R, Liu WM. Monitoring of temperature distribution in living biological tissues via blood perfusion. Eur Phys J Plus. 2012;127(8). doi:10.1140/epjp/i2012-12089-7
19. Hooshmand P, Moradi A, Khezry B. Bioheat transfer analysis of biological tissues induced by laser irradiation. International Journal of Thermal Sciences. 2015;90:214-223. doi:10.1016/j.ijthermalsci.2014.12.004
20. Kim S, Jeong S. Effects of temperature-dependent optical properties on the fluence rate and temperature of biological tissue during low-level laser therapy. Lasers Med Sci. 2013;29(2):637-644. doi:10.1007/s10103-013-1376-4
21. Wang Y, Liu J, Wang C, et al. Numerical analysis and experimental verification of time-dependent heat conduction under the action of ultra-short pulse laser. Front Phys. 2024;12. doi:10.3389/fphy.2024.1416064
22. Mignon C, Tobin DJ, Zeitouny M, Uzunbajakava NE. Shedding light on the variability of optical skin properties: finding a path towards more accurate prediction of light propagation in human cutaneous compartments. Biomed Opt Express. 2018;9(2):852. doi:10.1364/boe.9.000852
23. Baranoski GVG, Chen TF. Optical Properties of Skin Surface. Measuring the Skin. In: Humbert P, Fanian F, Maibach H, Agache P. (eds) Agache's Measuring the Skin. Springer, Cham. Doi:10.1007/978-3-319-26594-0_9-1
24. Setchfield K, Gorman A, Simpson AHRW, Somekh MG, Wright AJ. Relevance and utility of the in-vivo and ex-vivo optical properties of the skin reported in the literature: a review [Invited]. Biomed Opt Express. 2023;14(7):3555. doi:10.1364/boe.493588
25. Shimojo Y, Nishimura T, Hazama H, Ozawa T, Awazu K. Measurement of absorption and reduced scattering coefficients in Asian human epidermis, dermis, and subcutaneous fat tissues in the 400- to 1100-nm wavelength range for optical penetration depth and energy deposition analysis. J Biomed Opt. 2020;25(04):1. doi:10.1117/1.jbo.25.4.045002
26. Fu M, Weng W, Yuan H. Numerical Simulation of the Effects of Blood Perfusion, Water Diffusion, and Vaporization on the Skin Temperature and Burn Injuries. Numerical Heat Transfer, Part A: Applications. 2014;65(12):1187-1203. doi:10.1080/10407782.2013.869449
27. Ding H, Lu JQ, Wooden WA, Kragel PJ, Hu XH. Refractive indices of human skin tissues at eight wavelengths and estimated dispersion relations between 300 and 1600 nm. Phys Med Biol. 2006;51(6):1479-1489. doi:10.1088/0031-9155/51/6/008
28. Torvi DA, Dale JD. A Finite Element Model of Skin Subjected to a Flash Fire. Journal of Biomechanical Engineering. 1994;116(3):250-255. doi:10.1115/1.2895727
29. Ahmadikia H, Moradi A, Fazlali R, Parsa AB. Analytical solution of non-Fourier and Fourier bioheat transfer analysis during laser irradiation of skin tissue. J Mech Sci Technol. 2012;26(6):1937-1947. doi:10.1007/s12206-012-0404-9
30. Klanecek Z, Hren R, Simončič U, Muc BT, Lukač M, Milanič M. Finite Element Method (FEM) Modeling of Laser-Tissue Interaction during Hair Removal. Applied Sciences. 2023;13(14):8553. doi:10.3390/app13148553
31. Werner J, Buse M. Temperature profiles with respect to inhomogeneity and geometry of the human body. Journal of Applied Physiology. 1988;65(3):1110-1118. doi:10.1152/jappl.1988.65.3.1110
32. Zhou F, Wang Z, Guan D, Yang Y, Liu C. Human thermal responses under environmental step-change during different winter periods in severe cold area. Building and Environment. 2025;274:112770. doi:10.1016/j.buildenv.2025.112770
33. Huang YY, Sharma SK, Carroll J, Hamblin MR. Biphasic Dose Response in Low Level Light Therapy – an Update. Dose-Response. 2011;9(4). doi:10.2203/dose-response.11-009.hamblin
34. Bjordal JM. Low Level Laser Therapy (LLLT) and World Association for Laser Therapy (WALT) Dosage Recommendations. Photomedicine and Laser Surgery. 2012;30(2):61-62. doi:10.1089/pho.2012.9893
35. ÇİTKAYA AY, ŞEKER ŞS. Study of temperature distribution in light--tissue interaction using the FEM. Turk J Elec Eng & Comp Sci. 2016;24:807-819. doi:10.3906/elk-1307-95
36. Stebbing ARD. Hormesis – The stimulation of growth by low levels of inhibitors. Science of The Total Environment. 1982;22(3):213-234. doi:10.1016/0048-9697(82)90066-3
37. Hamblin MR, Demidova TN. Mechanisms of low level light therapy. Hamblin MR, Waynant RW, Anders J, eds. SPIE Proceedings. Published online February 9, 2006. doi:10.1117/12.646294
38. Jacques SL. Optical properties of biological tissues: a review. Phys Med Biol. 2013;58(11):R37-R61. doi:10.1088/0031-9155/58/11/r37
39. Joensen J, Demmink JH, Johnson MI, Iversen VV, Lopes-Martins RÁB, Bjordal JM. The Thermal Effects of Therapeutic Lasers with 810 and 904 nm Wavelengths on Human Skin. Photomedicine and Laser Surgery. 2011;29(3):145-153. doi:10.1089/pho.2010.2793
40. Tunér J, Hode L. It's All in the Parameters: A Critical Analysis of Some Well-Known Negative Studies on Low-Level Laser Therapy. Journal of Clinical Laser Medicine & Surgery. 1998;16(5):245-248. doi:10.1089/clm.1998.16.245